XXVI ENMC
ENCONTRO NACIONAL DE MODELAGEM COMPUTACIONAL
XIV ECTM
ENCONTRO DE CIÊNCIA E TECNOLOGIA DE MATERIAIS
2023

SIMULATION OF SURFACE TEMPERATURE DISTRIBUTION ON A BODY SUBJECTED TO EXTERNAL AIR FLOW

Leib de A. Neubarth[1] - leib999@yahoo.com.br
Norberto Mangiavacchi[1] - norberto@eng.uerj.br
José Pontes[1] - pontes.jose@gmail.com
Rachel M. Lucena[1] - rachel.lucena@eng.uerj.br
Hyun Ho Shin[1] - hshin@pol.una.py
André C. Martins[1] - amartins2295@gmail.com
[1]Universidade do Estado do Rio de Janeiro, Faculdade de Engenharia, Departamento de Engenharia Mecânica – Rio de Janeiro, RJ, Brazil

Abstract. *This article discusses the use of finite element-based CFD simulations to determine the temperature distribution on a body subjected to internal heating and forced convection. From a mathematical and computational standpoint, this problem requires the simultaneous resolution of various physical phenomena applied across distinct physical domains. Some challenges are addressed: equation nondimensionalization, coupling across different domains, and the stabilization of the finite element formulation of the Navier-Stokes equations.*

Keywords: *CFD, Finite Element Method, Heat Transfer, Multiphysics Problem*

1. INTRODUCTION

It is widely recognized that human beings are exothermic organisms, possessing the capacity for autoregulation of their corporeal temperature, thereby maintaining it within a delimited and particular range. When deviations from these established parameters occur, consequential issues tend to manifest. Hence, the temperature of the human body functions as an indicator of an individual's state of well-being, bearing documented records of its utilization dating back to the fifth century B.C. (Jiang et al., 2005)

For a long period, the contact thermometer stood as the sole apparatus competent in assessing human corporal temperature (Ring, 2014). However, contemporary advancements have facilitated the measurement through methodologies such as infrared (IR) thermography. Upon its application in the medical domain during the latter part of the 1950s, this technique garnered substantial attention within the field of medicine, owing to its non-invasive nature and its efficacy as a prominent indicator of physiological dysfunctions (Jiang et al., 2005). Furthermore, irregular temperature patterns can be readily discerned through infrared thermography, thereby facilitating the establishment of correlations with pathological

conditions, particularly in contexts of extensive screening, such as during pandemics (Fiscal et al., 2022).

The surface temperature distribution in the head is of particular interest for these applications and results from complex interplay of phenomena, mainly the geometry of the body, the airflow around the head, the convective heat transfer in the head and the conduction in the head. Ultimately, the surface temperature results in an infrared image that can be captured by an infrared camera. A computational model of the physical processes involved is of great value to improve the interpretation of this infrared image, providing basic tool for determination of the underlying causes of observed temperature variations.

In order to simulate the surface temperature distribution on a full 3D human head subjected to air flow, one simulation was done first: the flow around a 2D cylinder with inner heating. The former simulation was used to validate the multiphysics and multidomains code, while the latter was done to extend to code to 3 spacial dimensions.

Special attention was given to the interface between the fluid and solid domains. The heat transfer in it is done through convection by the fluid side and by conduction by the solid side. A penalty method was employed to couple the domains an will be described in the next session.

Finally, the solution of Navier-Stokes equations required the use of stabilization, since the Galerkin formulation for this problem is unstable. The Streamwise Upwind Petrov Galerkin (SUPG) and Pressure Stabilizing Petrov Galerkin (PSPG) schemes were used due to their consistency (Brooks & Hughes, 1982) (Tezduyar, 1991).

2. MATHEMATICAL MODELING

2.1 Problem formulation for a generic body with inner heating

The steady flow around an object at low speed is considered incompressible, and is modelled using the steady-state Navier-Stokes equations along with the continuity equation:

$$(\mathbf{u}\cdot\nabla)\mathbf{u} + \frac{1}{\rho}\nabla p - \frac{\mu}{\rho}\nabla^2\mathbf{u} = \mathbf{0} \qquad \text{in } \Omega_f, \tag{1a}$$

$$\nabla\cdot\mathbf{u} = 0 \qquad \text{in } \Omega_f, \tag{1b}$$

where $\mathbf{u}$ is the fluid velocity field, p is the fluid pressure field, μ is the fluid dynamic viscosity, ρ the fluid density and Ω_f is the fluid domain.

The boundary conditions of the problem for the velocity and pressure are:

$$\begin{cases} \mathbf{u} = \mathbf{u_{in}} & \text{on } \Gamma_{in}\cup\Gamma_{top}, \\ \mathbf{u} = \mathbf{0} & \text{on } \Gamma_{cyl}, \\ \mathbf{n}\cdot\nabla\mathbf{u} = \mathbf{0} & \text{on } \Gamma_{fN} = \Gamma_{sym}, \\ p = 0 & \text{on } \Gamma_{out}, \end{cases} \tag{2}$$

where $\mathbf{u_{in}}$ is a prescribed inlet velocity and also the Dirichlet condition for the top boundary and $\mathbf{n}$ is the outward normal vector.

Besides that, the temperature of the medium is also taken into account. Within the fluid domain Ω_f the temperature field is described by a steady advection-diffusion equation (Eq. (3a)). Within the solid domain Ω_s the velocity $\mathbf{u}$ is zero; therefore, the temperature follows

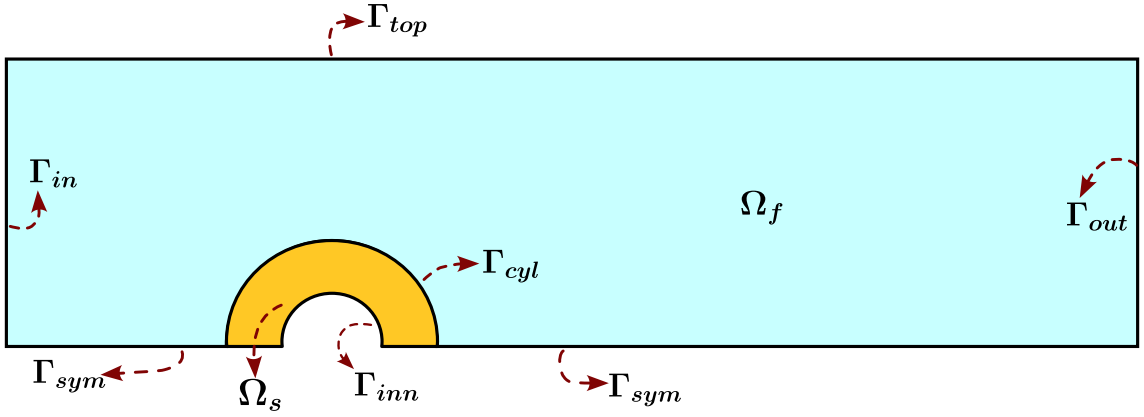

Figure 1: Simplified sketch of domains and boundaries in the 2D problem.

a purely steady diffusive process (Eq. (3b)):

$$\mathbf{u} \cdot \nabla T_f - \nabla \cdot (\alpha_f \nabla T_f) = 0 \qquad \text{in } \Omega_f, \tag{3a}$$

$$\nabla \cdot (\alpha_s \nabla T_s) = 0 \qquad \text{in } \Omega_s, \tag{3b}$$

where α_f and α_s are the thermal diffusivities in the fluid and solid domains, and T_f and T_s the temperature field in the fluid and solid domains, respectively.

The boundary conditions of the problem for the temperature are:

$$\begin{cases} T = T_{in} & \text{on } \Gamma_{in}, \\ T = T_{inn} & \text{on } \Gamma_{inn}, \\ \mathbf{n} \cdot \nabla T = 0 & \text{on } \Gamma_{sN} = \Gamma_{sym} \cup \Gamma_{top} \cup \Gamma_{out}, \end{cases} \tag{4}$$

and the interface condition is:

$$T_s = T_f \qquad \text{on } \Gamma_{cyl}. \tag{5}$$

Although Eqs. (1a)-(5) govern the phenomena, they are not used in the way they were presented. First, a procedure of non-dimensionalization was carried. Such approach brings many advantages, such as simplification, comparability, dimensional consistency, insight into dominant factors and greater numerical stability.

2.2 Non-dimensionalization of Navier-Stokes equations

By choosing a characteristic length L_0 and speed u_0, it is possible to rewrite the Eqs. (1a) and (1b) in a non-dimensional manner. This is done applying a variable change for the velocity $\mathbf{u}$ and the position x, using the following non-dimensional forms $\mathbf{u}^*$ and x_i^*, defined in (6):

$$\mathbf{u}^* = \frac{\mathbf{u}}{u_0}; \qquad\qquad x_i^* = \frac{x_i}{L_0}. \tag{6}$$

Using the new variables defined in (6) the Eqs. (1a) and (1b) become:

$$(\mathbf{u}^* \cdot \nabla^*)\mathbf{u}^* + \nabla^* p^* - \frac{1}{Re}\nabla^{*2}\mathbf{u}^* = \mathbf{0} \tag{7a}$$

$$\nabla^* \cdot \mathbf{u}^* = 0. \tag{7b}$$

In Eqs. (7a) and (7b) the operators ∇^*, $\nabla^* \cdot$ and ∇^{*2} denote the gradient, divergent and laplacian according to the new non-dimensional coordinates x_i^*. p^* is a new variable defined by Eq. (8a) and Re is the non-dimensional Reynolds number, as in Eq. (8b):

$$p^* = \frac{p}{\rho u_0^2} \tag{8a}$$

$$Re = \frac{\rho\ u_0\ L_0}{\mu}. \tag{8b}$$

2.3 Non-dimensionalization of scalar advection-diffusion equation

In order to carry out the process of non-dimensionalization on Eqs. (3a) and (3b), we utilize the identical characteristic length L_0 and speed u_0 as introduced in (6). Additionally, a non-dimensional temperature denoted as T^* is formulated. This formulation involves the two boundary condition temperatures T_{in} and T_{inn}, hence

$$T^* = \frac{T - T_{in}}{T_{inn} - T_{in}}, \tag{9a}$$

$$Pr = \frac{\mu}{\rho\alpha}. \tag{9b}$$

Employing the new variables defined in Eqs. (6), (9a), and the non-dimensional numbers Reynolds (Eq. (8b)) and Prandtl (Eq. (9b)) the equations (3a) and (3b) become:

$$\mathbf{u}^* \cdot \nabla^* T^* - \frac{1}{Re\ Pr} \nabla^{*2} T^* = 0, \tag{10a}$$

$$\nabla^{*2} T^* = 0. \tag{10b}$$

For enhanced clarity, henceforth the asterisk symbol representing a non-dimensional variable/operator will be omitted for improved readability. In the subsequent sections, solely the non-dimensional form will be employed.

2.4 Finite Element Method formulation

In the simulations, both inf-sup P_k/P_{k-1} stable velocity-pressure pair and P_k/P_k were used, with continuous velocities and pressures. In the first case, the velocity interpolation space V for the fluid domain is defined as follows:

$$V \doteq \{\mathbf{v} \in [H^1(\Omega_f)]^d :\ \mathbf{v}|_c \in [P_k(c)]^d \text{ for all } c \in \mathcal{T}_f\}, \tag{11}$$

where $\mathbf{v}$ is the test function belonging to a Hilbert space H^1 defined on the domain Ω_f such that $\mathbf{v}$ in each cell c of the triangulation $\mathcal{T}_f$ defined over the domain Ω_f belongs to the cell polinomial vector space $[P_k(c)]^d$. k is the order of the polinomial used to interpolate the element.

The pressure interpolation space Q for the fluid domain is:

$$Q \doteq \{q \in C^0(\Omega_f) :\ q|_c \in P_{k-1}(c) \text{ for all } c \in \mathcal{T}_f\}, \tag{12}$$

where q is the test function and C^0 the space of continuous functions without continuous derivatives. The temperature interpolation spaces R_X are similar to the pressure interpolation space:

$$R_X \doteq \{r_X \in C^0(\Omega_X) :\ r_X|_c \in P_{k-1}(c) \text{ for all } c \in \mathcal{T}_X\}. \tag{13}$$

The definition in Eq. (13) actually defines two spaces: R_f for the fluid domain and R_s for the solid domain. Replacing the X subindex by f or s gives the definition for the fluid or solid domain, respectively. In order to implement Eqs. (7a), (7b), (10a) and (10b) using the finite element method, these equations must be put in the weak form. The weak form for this equations is:

$$\int_{\Omega_f} \mathbf{v} \cdot (\mathbf{u} \cdot \nabla \mathbf{u})\, d\Omega_f + \frac{1}{Re} \int_{\Omega_f} \nabla \mathbf{u} : \nabla \mathbf{v}\, d\Omega_f - \int_{\Omega_f} p \nabla \cdot \mathbf{v}\, d\Omega_f - \frac{1}{Re} \int_{\Gamma_f N} \mathbf{v} \cdot (\nabla \mathbf{u} \cdot \mathbf{n})\, d\Gamma_f N = \mathbf{0}, \tag{14a}$$

$$\int_{\Omega} q \nabla \cdot \mathbf{u}\, d\Omega_f = 0, \tag{14b}$$

$$\int_{\Omega_f} r_f\, (\mathbf{u} \cdot \nabla T_f)\, d\Omega_f - \frac{1}{RePr} \left(\int_{\Gamma_{fN}} r_f (\nabla T_f \cdot \mathbf{n})\, d\Gamma_{fN} - \int_{\Omega_f} \nabla T_f \cdot \nabla r_f\, d\Omega_f \right) = 0, \tag{14c}$$

$$\int_{\Gamma_{sN}} r_s (\nabla T_s \cdot \mathbf{n})\, d\Gamma_{sN} + \int_{\Omega_s} \nabla T_s \cdot \nabla r_s\, d\Omega_s = 0, \tag{14d}$$

where Γ_{fN} and Γ_{sN} are the subsets of the fluid and solid boundaries which are subject to Neumann conditions.

2.5 Navier-Stokes Stabilization

As presented in Eq. (14a), the Galerkin finite element aproximation Navier-Stokes equations is unstable. One way of stabilizing them is through the use of a stabilization scheme. The chosen scheme was the SUPG - Streamwise Upwind Petrov Galerkin - for the velocity stabilization and PSPG - Pressure Stabilization Petrov Galerkin - for pressure. The idea behind this schemes is to add diffusion to the flow in its streamwise direction. This is accomplished by chosing different test functions: $\mathbf{u} \cdot \nabla \mathbf{v}$ for velocity and ∇q for pressure, which are multiplied by the Navier-Stokes differential operator $L(\mathbf{u}, p)$ (Eq. (15e)). More details can be found in (Tezduyar, 1991).

$$R_{NS}(\mathbf{u}, p) = \int_{\Omega_f} \mathbf{v} \cdot (\mathbf{u} \cdot \nabla \mathbf{u})\, d\Omega_f + \frac{1}{Re} \int_{\Omega_f} \nabla \mathbf{u} \cdot \nabla \mathbf{v}\, d\Omega_f - \int_{\Omega_f} p \nabla \cdot \mathbf{v}\, d\Omega_f - \frac{1}{Re} \oint_{\Gamma_f N} \mathbf{v} \cdot (\nabla \mathbf{u} \cdot \mathbf{n})\, d\Gamma_f N, \tag{15a}$$

$$R_{SUPG}(\mathbf{u}, p) = \int_{\Omega_f} \tau \cdot (\mathbf{u} \cdot \nabla \mathbf{v}) \cdot L(\mathbf{u}, p)\, d\Omega_f, \tag{15b}$$

$$R_{PSPG}(\mathbf{u}, p) = \int_{\Omega_f} \tau \cdot (\nabla q) \cdot L(\mathbf{u}, p) + \tau \cdot (\mathbf{u} \cdot \mathbf{u})(\nabla \cdot \mathbf{v})(\nabla \cdot \mathbf{u})\, d\Omega_f, \tag{15c}$$

$$R_{total1}(\mathbf{u}, p) = R_{NS}(\mathbf{u}, p) + R_{SUPG}(\mathbf{u}, p) + R_{PSPG}(\mathbf{u}, p), \tag{15d}$$

$$L(\mathbf{u}, p) = (\mathbf{u} \cdot \nabla)\mathbf{u} + \nabla p - \frac{1}{Re} \nabla^2 \mathbf{u}. \tag{15e}$$

Using this stabilization, is possible to use functional spaces P_k/P_k, such as P_1/P_1, which results in very low memory requirements and faster processing times when compared to the P_2/P_1.

The total residual R_{total1} is the sum of the Navier-Stokes weak form residual R_{NS} weighted by the Galerkin method plus the SUPG and PSPG residuals. From this expression a system is assembled; them, the velocity and pressure fields are calculated in the fluid domain. Then, the temperature field in both domains is coupled using the penalty method.

2.6 Domains temperature coupling

In the Γ_{cyl} surface, there is a interface between the fluid and solid domains Ω_f and Ω_s. The temperature in this interface is imposed through a penalty added to the residuals of the equations modeling each domain:

$$R_{T_f}(T_f) = \int_{\Omega_f} r_f \, (\mathbf{u} \cdot \nabla T_f) \, d\Omega_f - \frac{1}{RePr} \oint_{\Gamma_{fN}} r_f (\nabla T_f \cdot \mathbf{n}) \, d\Gamma_{fN} + \frac{1}{RePr} \int_{\Omega_f} \nabla T_f \cdot \nabla r_f \, d\Omega_f, \tag{16a}$$

$$R_{T_s}(T_s) = \oint_{\Gamma_{sN}} r_s (\nabla T_s \cdot \mathbf{n}) \, d\Gamma_{sN} - \int_{\Omega_s} \nabla T_s \cdot \nabla r_s \, d\Omega_s, \tag{16b}$$

$$R_i(T_f, T_s) = \int_{\Gamma_{cyl}} \gamma (T_{f+} - T_{s-})(r_{f+} - r_{s-}) \, d\Gamma_{cyl}, \tag{16c}$$

$$R_{total2}(T_f, T_s) = R_{T_f}(T_f) + R_{T_s}(T_s) + R_i(T_f, T_s). \tag{16d}$$

Equations (16a) and (16b) are the residuals for the weak forms defined in Eqs. (14c) and (14d). Equation (16c) is the interface coupling: a constant parameter γ set to 10^5 times two jump conditions. This conditions weakly enforce that the trial and test functions of both domains are the same on the interface, assuring the continuity of the solution across the interface.

2.7 Cylinder Simulation

To validate the mathematical development presented, the first problem solved is the flow past a cylinder with an inner heating. The meshes for this problem were entirely made in GMSH, an open source and free mesh generator (Geuzaine & Remacle, 2009). Both 2D and 3D simulations were performed. The 2D mesh has $131,282$ triangles, and the 3D mesh has $351,673$ tetrahedra.

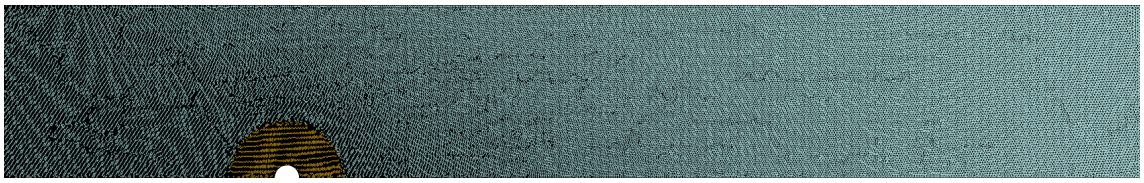

Figure 2: Mesh used in the 2D cylinder simulation.

The boundary conditions used were those shown in Eqs. (2), (4) and (5). The nondimensional values were:

$$\begin{cases} T_{in} = 0.0, \\ T_{inn} = 1.0, \\ \mathbf{u_{in}} = (1, 0). \end{cases} \tag{17}$$

u_0 was set to 1 m/s to found the boundary condition of $\mathbf{u}$. T_{in} and T_{inn} were calculated from Eq. (9a). They represent 25°C and 38°C, respectively.

2.8 3D Head Simulation

The airflow around the head was simulated using a 3D mesh. This mesh was built from an STL model. Three software were used: Blender (Community, 2018), Salome and GMSH (Geuzaine & Remacle, 2009).

Blender is an open source 3D editor and was used to cut the model in half. This was done to reduce CPU processing time and RAM memory requirements. Besides being cut in half, an internal cylinder was cut to prepare the simulation for a future experimental validation. This internal cylinder will be replaced by a heating resistance, and in the simulation it was modeled as the Dirichlet surface Γ_{inn}. The fluid domain around the head is meant to simulate a wind tunnel.

Salome was used to create the tetrahedral external and internal mesh. In this context of the 3D simulation, the external mesh is the fluid domain Ω_f and the internal mesh is the solid domain Ω_s.

Finally, GMSH was used to label all physical surfaces and domains, and to export the mesh to a suitable format for the FEM code. The labels and boundary conditions in 3D are homologous to the in 2D, with few changes.

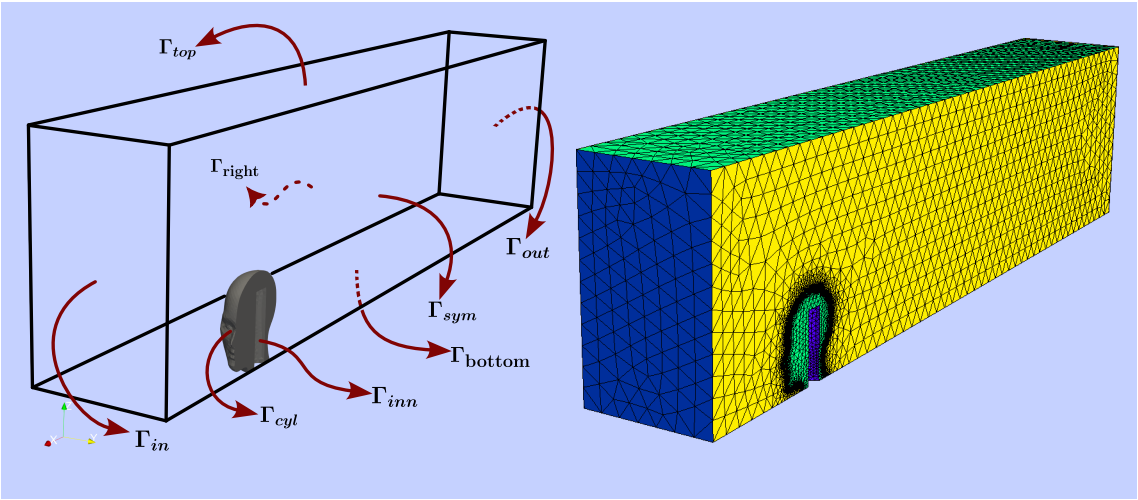

Figure 3: 3D domains discretization. Left: simplified representation of boundaries in the 3D problem. Right: 3D mesh used in the simulations.

The velocity and pressure boundary conditions for the 3D problem are almost the same as for the 2D problem, with 2 new boundaries: Γ_{right} and Γ_{bottom}. They have Dirichlet conditions, specified in Eq. (18):

$$\begin{cases} \mathbf{u} = \mathbf{u_{in}} & \text{on } \Gamma_{in} \cup \Gamma_{top} \cup \Gamma_{right}, \\ \mathbf{u} = \mathbf{0} & \text{on } \Gamma_{cyl} \cup \Gamma_{bottom}, \\ \mathbf{n} \cdot \mathbf{u} = 0 & \text{on } \Gamma_{fN} = \Gamma_{sym}, \\ p = 0 & \text{on } \Gamma_{out}. \end{cases} \tag{18}$$

The conditions for temperature are the same as for the 2D case (Eq. (4)). The FEM code

	Simulation	Experiment from (Taneda et al., 1956)
non dimensional vortex length s/d	2.25	2.1
stagnation point angle θ	50.6	53

Table 1: Comparison between simulation and experimental data.

was implemented using Gridap, which made possible to use the same mathematical formulation and code from the 2D case for the 3D simulation.

3. RESULTS

3.1 2D Cylinder

In Fig. 5 the velocity and temperature fields calculated for the 2D cylinder are shown. In order to validate this results, data gathered from (Taneda et al., 1956) was used. From Fig. 4 the vortex length s and separation angle θ were measured. The results - shown in Table 1 - are in good agreement with the literature.

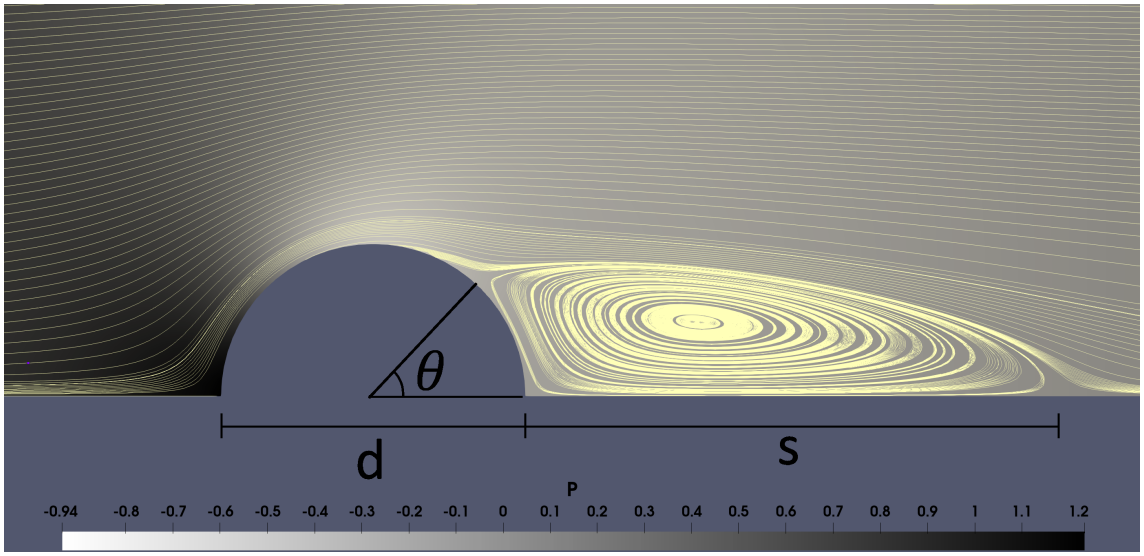

Figure 4: Vortex formation downstream the 2D cylinder. Pressure field in the background behind the streamlines.

3.2 3D Head

The flow velocity, temperature and pressure of Ω_f were found. The temperature in Ω_s (Fig. 7) was also obtained. In Fig. 6, a horizontal plane in the height of the eyes was cut to compare the 3D result to that from Fig. 5.

Since the code in Gridap running the 3D simulation was the same as the 2D case with minor changes in the boundary conditions, is assumed that the 2D experimental validation is valid for the 3D simulation.

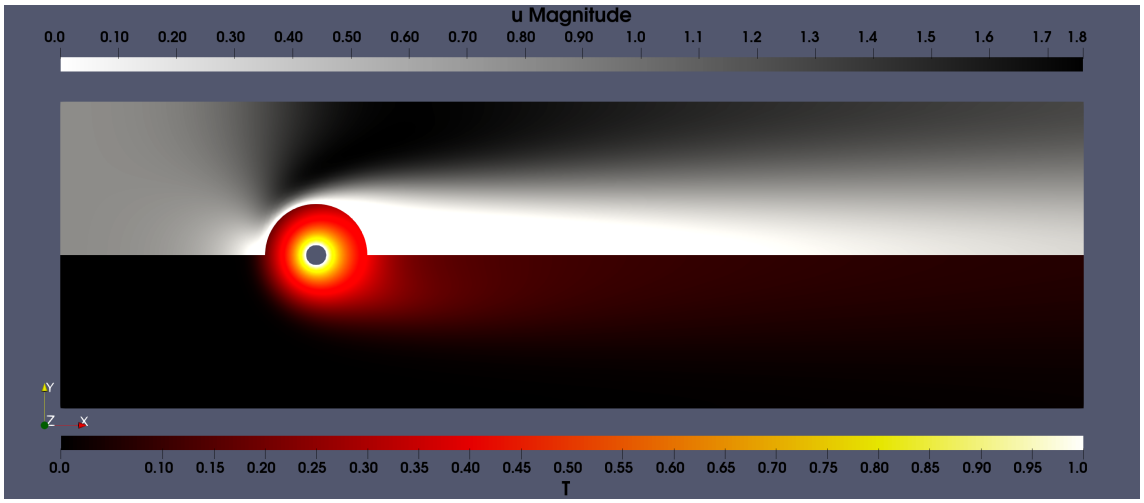

Figure 5: 2D cylinder simulation results. Top half: velocity field in Ω_f. Center and bottom half: temperature fields in Ω_s and Ω_f.

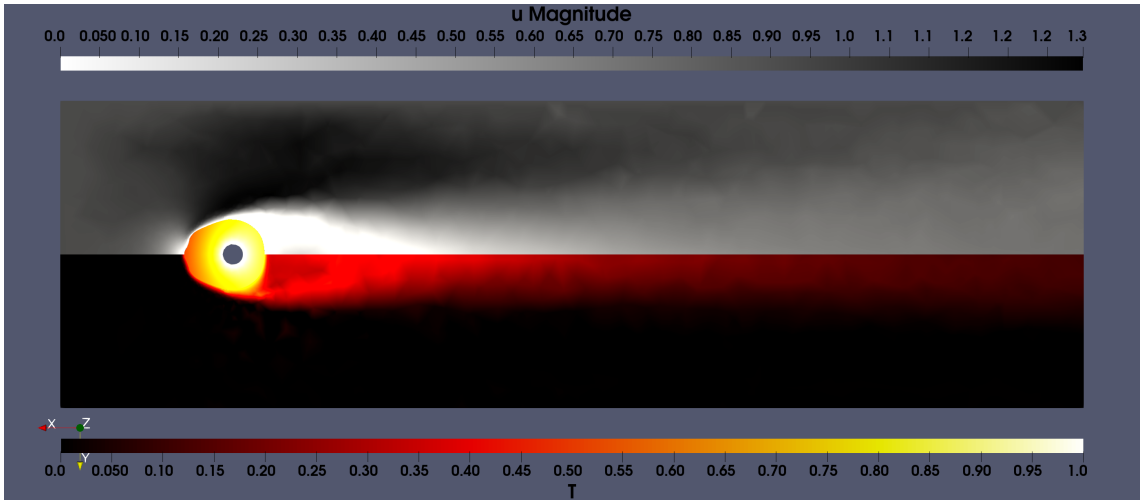

Figure 6: 3D simulation results: top view with a clip on the eyes plane. Top half: velocity field in Ω_f. Center and bottom half: temperature fields in Ω_s and Ω_f.

4. CONCLUSIONS

This paper aimed to simulate the temperature distribution in a face. A proper finite element formulation was implemented to simulate the Navier-Stokes equations and the scalar advection and diffusion equation. This formulation was able to link the temperature between multiple mathematical, physical and computational domains. The 2D code was validated using experimental data from the literature, and in future works the 3D simulations are expected to be tested against a wind tunnel experiment.

Acknowledgements

The authors would like to acknowledge financial support from FAPERJ, CAPES and CNPq.

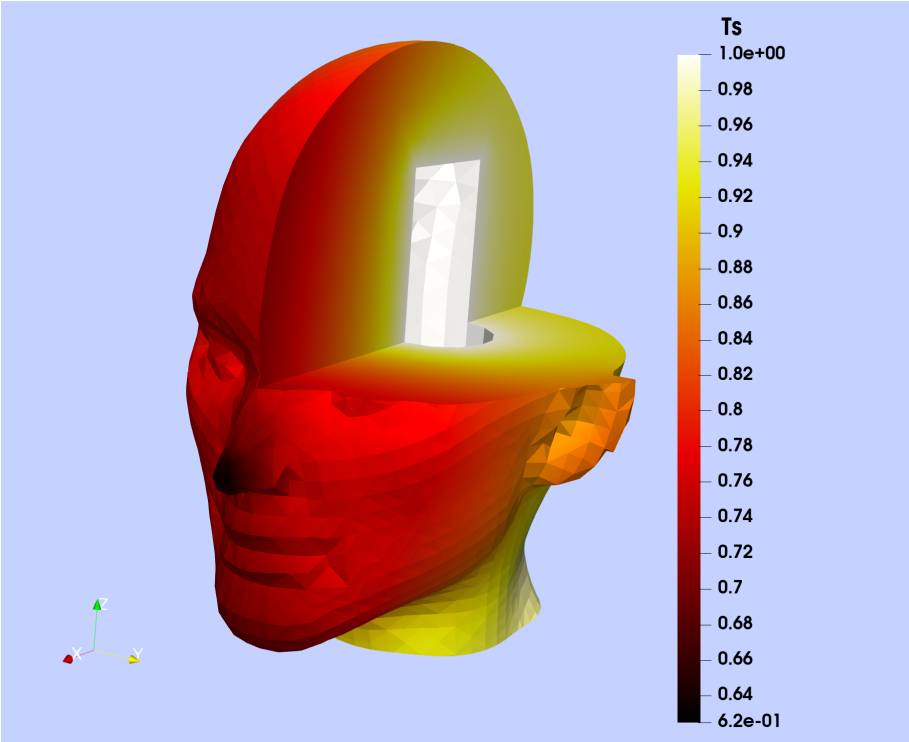

Figure 7: 3D simulation results: head surface and interior.

REFERENCES

Jiang, LJ and Ng, EYK and Yeo, ACB and Wu, S and Pan, F and Yau, WY and Chen, JH and Yang, Y. (2005), "A perspective on medical infrared imaging", *Journal of medical engineering & technology*, vol 29, n 6, 257-267.

Ring, F.J. (2014), "Pioneering progress in infrared imaging in medicine", *Quantitative InfraRed Thermography Journal*, vol 11, n 1, 57-65.

Fiscal, MRC and Treviño, V and Treviño, LJR and López, RO and Huerta, SC and Lara-Díaz, VJ and Peña, JGT. (2022), "COVID-19 classification using thermal images", *Journal of Biomedical Optics*, vol 27, 1-19.

Tezduyar, T. (1991), Stabilized Finite Element Formulations for Incompressible Flow Computations. *Advances In Applied Mechanics*. pp. 1-44.

Geuzaine, C. & Remacle, J. (2009), Gmsh: A 3-D finite element mesh generator with built-in pre- and post-processing facilities. *International Journal For Numerical Methods In Engineering*. **79**, 1309-1331.

Community, B. (2018), Blender - a 3D modelling and rendering package. (Blender Foundation,2018), http://www.blender.org.

Brooks, A. & Hughes, T. (1982), Streamline upwind/Petrov-Galerkin formulations for convection dominated flows with particular emphasis on the incompressible Navier-Stokes equations. *Computer Methods In Applied Mechanics And Engineering*. **32**, 199-259.

Taneda, S. (1956), Experimental Investigation of the Wakes behind Cylinders and Plates at Low Reynolds Numbers. *Journal Of The Physical Society Of Japan*. **11**, 302-307.